High-Resolution Mapping of Nitrogen Dioxide With TROPOMI: First Results and Validation Over the Canadian Oil Sands

Debora Griffin[1] (ID), Xiaoyi Zhao[1], Chris A. McLinden[1] (ID), Folkert Boersma[2,3] (ID), Adam Bourassa[4] (ID), Enrico Dammers[1], Doug Degenstein[4], Henk Eskes[2], Lukas Fehr[4] (ID), Vitali Fioletov[1], Katherine Hayden[1], Shailesh K. Kharol[1] (ID), Shao-Meng Li[1], Paul Makar[1], Randall V. Martin[5] (ID), Cristian Mihele[1], Richard L. Mittermeier[1], Nickolay Krotkov[6] (ID), Maarten Sneep[2], Lok N. Lamsal[6,7] (ID), Mark ter Linden[2,8], Jos van Geffen[2] (ID), Pepijn Veefkind[2,9], and Mengistu Wolde[1,10]

[1]Air Quality Research Division, Environment and Climate Change Canada, Toronto, Ontario, Canada, [2]Royal Netherlands Meteorological Institute (KNMI), De Bilt, The Netherlands, [3]Environmental Sciences Group, Wageningen University, Wageningen, The Netherlands, [4]Institute of Space and Atmospheric Studies, University of Saskatchewan, Saskatoon, Saskatchewan, Canada, [5]Department of Physics and Atmospheric Science, Dalhousie University, Halifax, Nova Scotia, Canada, [6]Laboratory for Atmospheric Chemistry and Dynamics, NASA Goddard Space Flight Center, Greenbelt, MD, USA, [7]Goddard Earth Sciences Technology and Research, Universities Space Research Association, Columbia, MD, USA, [8]Science and Technology (S&T), Delft, Netherlands, [9]Department of Civil Engineering and Geosciences, Delft University of Technology, Delft, Netherlands, [10]National Research Council Canada, Flight Research Laboratory, Ottawa, Canada

Abstract TROPOspheric Monitoring Instrument (TROPOMI), on-board the Sentinel-5 Precurser satellite, is a nadir-viewing spectrometer measuring reflected sunlight in the ultraviolet, visible, near-infrared, and shortwave infrared. From these spectra several important air quality and climate-related atmospheric constituents are retrieved, including nitrogen dioxide (NO$_2$) at unprecedented spatial resolution from a satellite platform. We present the first retrievals of TROPOMI NO$_2$ over the Canadian Oil Sands, contrasting them with observations from the Ozone Monitoring Instrument satellite instrument, and demonstrate TROPOMI's ability to resolve individual plumes and highlight its potential for deriving emissions from individual mining facilities. Further, the first TROPOMI NO$_2$ validation is presented, consisting of aircraft and surface in situ NO$_2$ observations, and ground-based remote-sensing measurements between March and May 2018. Our comparisons show that the TROPOMI NO$_2$ vertical column densities are highly correlated with the aircraft and surface in situ NO$_2$ observations, and the ground-based remote-sensing measurements with a low bias (15–30 %); this bias can be reduced by improved air mass factors.

Plain Language Summary Nitrogen dioxide (NO$_2$) is a pollutant that is linked to respiratory health issues and has negative environmental impacts such as soil and water acidification. Near the surface the most significant sources of NO$_2$ are fossil fuel combustion and biomass burning. With a recently launched satellite instrument (TROPOspheric Monitoring Instrument [TROPOMI]), NO$_2$ can be measured with an unprecedented combination of accuracy, spatial coverage, and resolution. This work presents the first TROPOMI NO$_2$ measurements near the Canadian Oil Sands and shows that these measurements have an outstanding ability to detect NO$_2$ on a very high horizontal resolution that is unprecedented for satellite NO$_2$ observations. Further, these satellite measurements are in excellent agreement with aircraft and ground-based measurements.

1. Introduction

The ability to observe the near-surface abundance of air pollutants from space has drastically increased over the last two decades. The first space-borne ultraviolet-visible spectrometer focusing on the tropospheric composition was the Global Ozone Monitoring Experiment (GOME), 1995–2011, with a pixel size of 40 × 320 km^2 (Burrows et al., 1999), followed by the SCanning Imaging Absorption SpectroMeter for Atmospheric

Cartography (SCIAMACHY), 2002–2012 ($30 \times 60\,km^2$; Bovensmann et al., 1999) and the GOME-2 instruments (2006–present, 2012–present; $40 \times 40/80\,km^2$; Callies et al., 2000). Until now, the previous standard was the Ozone Monitoring Instrument (OMI; 2004–present; $13 \times 24\,km^2$; at nadir; Krotkov et al., 2016; Levelt et al., 2006), which was able to resolve pollutant distributions at the urban scale (20–30 km), and from which emissions could be inferred for large point sources (e.g., de Foy et al., 2015; Ghude et al., 2013; Lu & Streets, 2012). However, with the launch of the European Space Agency's Sentinel-5 Precurser (S5P) on 13 October 2017, space-borne measurements have entered a new era. In addition to spatial resolution, data product quality of the recorded spectra has significantly increased for this type of space-borne UV-vis spectrometer over the past two decades.

Here we focus on the first retrieval results of tropospheric NO_2 from TROPOMI. NO_2 is an important pollutant gas that is linked to respiratory health issues (Health Canada, 2018) and has negative environmental impacts such as soil and water acidification (Environment Canada, 2018). Nitrogen monoxide (NO) is emitted by combustion processes, such as fossil fuel combustion and biomass burning, as well as lightning, where molecular nitrogen (N_2) combines with molecular oxygen (O_2) at extremely high temperatures. NO is then rapidly oxidized to form NO_2. Due to the rapid cycling between them, NO and NO_2 are often considered together as NO_x ($NO+NO_2$). Within a plume, the lifetime of NO_x is relatively short, on the order of a few hours, and is in daytime primarily removed by reaction with the hydroxyl radical (OH). Due to this short lifetime, background NO_2 concentrations can be orders of magnitude smaller than levels near polluted areas.

This study presents the first TROPOMI tropospheric NO_2 retrievals (offline v.101; Boersma et al., 2018; van Geffen et al., 2018) and demonstrates TROPOMI's ability to resolve individual plumes from space at a spatial resolution several times better than the previous best from OMI (roughly a factor of 15). To demonstrate the quality of the TROPOMI NO_2 product and its suitability for high-resolution mapping, aircraft and ground-based data over the Athabasca Oil Sands Region (AOSR) in northeastern Alberta, Canada, are used for its evaluation. The AOSR, and in particular the surface mining area at 57° N, is a remote area that has significant NO_x emissions from from a variety of types of industrial sources, such as upgraders (a facility that converts bitumen, a viscous form of oil found in the oil sands, into synthetic crude oil) and heavy transportation vehicles (McLinden et al., 2012; Percy et al., 2012). As such, this region is an ideal location for evaluating the TROPOMI NO_2 retrieval product and its ability to capture localized enhancements of NO_2, including individual plumes, and low background values over a relatively small domain. We also contrast these results with a similar analysis of lower resolution OMI observations to help demonstrate the importance of the finer spatial resolution in capturing horizontal gradients and small-scale features.

2. Datasets

2.1. Satellite NO_2 Data

TROPOMI is the single payload on the S5P satellite that has a Sun-synchronous orbit with a local overpass time of around 1:30 pm and has near full-surface coverage on a daily basis (Hu et al., 2018; Veefkind et al., 2012). The instrument contains four spectrometers: three that cover the ultraviolet-near infrared with two spectral bands at 270–500 nm and 675–775 nm, and one for the shortwave infrared. The TROPOMI NO_2 retrieval algorithm was developed by the Royal Netherlands Meteorological Institute and utilizes the bands of the ultraviolet-near infrared spectrometer (405–465 nm). The retrieval algorithm is based on the NO_2 DOMINO retrieval previously used for OMI spectra (Boersma et al., 2011) with improvements made for all retrieval substeps (Lorente et al., 2017; van Geffen et al., 2015; Zara et al., 2018) within the QA4ECV project (Boersma et al., 2018; van Geffen et al., 2018). A tropospheric vertical column density (VCD, or simply "column") is provided by the algorithm, which represents the vertically integrated number of NO_2 molecules per unit area between the surface and the tropopause (in units of mol/m^2, with typical columns ranging globally from 10–200 $\mu mol/m^2$). The precision is also provided, which ranges from approximately 30–40 % and 75–100 % for snow-free and snow-covered surfaces, respectively. To determine the crucial air mass factor (AMF), a measure of the measurement's sensitivity (e.g., McLinden et al., 2014; Palmer et al., 2001), the profile shape of the TM5-MP model is used (at $1 \times 1°$ resolution; Williams et al., 2017); the surface albedo information is derived from a monthly OMI climatology (on a $0.5 \times 0.5°$ resolution; Kleipool et al., 2008. TROPOMI uses a snow flag from the Near real-time Ice and Snow Extent (NISE), and the albedo is set to 0.6 (over the AOSR) if the surface beneath is covered in snow or ice. Aerosol was not included in the AMF calculation as aerosol optical depths are modest in the oil sands at 0.1–0.2 (Sioris et al., 2017), and there

AGU
100
ADVANCING EARTH
AND SPACE SCIENCE

Geophysical Research Letters

10.1029/2018GL081095

are somewhat offsetting impacts when they are omitted from both cloud retrievals and AMF calculations (Boersma et al., 2004). For this study we use v1.01 (van Geffen et al., 2018), the first released offline version of the TROPOMI tropospheric NO_2 columns (https://s5phub.copernicus.eu; http://www.tropomi.eu). Spatial resolution varies with across-track position, and in this study the average pixel size is $6 \times 7\,km^2$. Pixels that are fully or partially covered by clouds were filtered; here we used 0.3 as a cutoff for the radiative cloud fraction ("cloud_fraction_crb_nitrogendioxide_window").

OMI NO_2 observations (NASA Standard Product, SP, version 3.1; Krotkov et al. 2017; Marchenko et al. 2015) are used in order to evaluate the relative performance of TROPOMI and OMI. The OMI data are filtered in a similar manner as TROPOMI with an additional restriction that only smaller pixels are considered (track positions 11–50), which are automatically removed in the SPv3.1 product.

2.2. In Situ Measurements

Aircraft-borne in situ measurements were taken in April 2018 over the AOSR as part of Environment and Climate Change Canada's aircraft campaign. Here we use measurements taken during three flights, on 5, 9, and 13 April 2018 between 16:30 and 21:00 UTC. The TROPOMI overpasses in this region are typically between 19:00 and 21:00 UTC; on some days two overpasses occur that are approximately 100 min apart. During those flights, air parcels were sampled in the planetary boundary layer (PBL) between approximately 200 and 400 m agl (above ground level) with occasional spiral flights reaching up to 2,300 m agl.

The aircraft in situ NO_2 measurements were taken on-board a National Research Council of Canada's Convair 580 research aircraft using two Thermo Scientific Model 42i-TL ($NO–NO_2–NO_x$) Analyzers, modified to measure at 1-Hz time resolution. The first analyzer measured NO directly, while the second analyzer measured the sum of NO and large fraction of NO_2 (65%), selectively converted to NO using a photolytic converter (Air Quality Design Inc.). NO_2 was then calculated by difference and averaged to 3 s, with an estimated detection limit of 0.2 ppbv and an uncertainty of 3 % of the reported value +0.4 ppbv.

Ground-based NO_2 in situ concentrations are continuously sampled at 17 locations in northeastern Alberta as part of the Wood Buffalo Environment Association (WBEA; http://wbea.org/historical-monitoring-data/; Percy et al., 2012). NO_2 concentrations (measured in a similar way as described above for the aircraft measurements; see supporting information; Hsu et al., 2010; Percy, 2013; Phillips, 2010; U.S. Environmental Protection Agency, 1975) are available every 5 min.

2.3. Pandora Instrument

A type of ground-based spectrometer, known as Pandora, has been developed to help evaluate satellite NO_2 retrievals (Herman et al., 2009). The Pandora instrument measures direct sunlight in the UV-vis spectral range (280–525 nm). High-quality NO_2 total columns (tropospheric + stratospheric) are obtained by using the differential optical absorption spectroscopy technique (Noxon, 1975; Platt & Stutz, 2008) in 400- to 440-nm range. The retrieved NO_2 total columns data have a precision of $\pm2.7 \times 10^{14}$ molec/cm^2 (Herman et al., 2009). A Pandora instrument has been deployed in Fort McKay in the AOSR (57.184° N, 111.64° W) since 2013 (Fioletov et al., 2016). NO_2 columns are available approximately every 1.5 min under unobscured Sun conditions.

2.4. GEM-MACH

In this study we utilize the NO_2 profile shape from Environment and Climate Change Canada's air quality forecast model: the Global Environmental Multiscale-Modelling Air-quality and Chemistry (GEM-MACH). The operational version of the model (Moran et al., 2010; Pendlebury et al., 2018) has a $10 \times 10\,km^2$ grid cell size for North American domain, 80 vertical levels (from the surface to approximately 0.1 hPa). The operational forecast makes use of 2013 emissions information (Zhang et al., 2018). Here we use the daily model output for the closest hour of the measurements and the closest grid box of the 10-km resolution version of GEM-MACH between 0 and 1.5 km. Between 1.5 and 12 km, we use concentrations from a monthly GEOS-Chem (Bey et al., 2001) model run at the approximate TROPOMI overpass time, as the GEM-MACH model currently does not include NO_x sources in the free troposphere, such as lightning and aircraft emissions. Further details can be found in the supporting information (Akingunola et al., 2018; Coats, 1996; Côté et al., 1998; Girard et al., 2014; Makar, Gong, Milbrandt, et al., 2015, Makar, Gong, Hogrefe, et al., 2015).

2.5. Alternative AMF

The measurements shown here were taken between March and May 2018, and for much of this period the surface was snow covered (note that data for March is preoperational and may be slightly noisier).

In principle, this highly reflective surface enables a more accurate retrieval with larger signals and less dependence on the knowledge of profile shape (e.g., McLinden et al., 2014; O'Byrne et al., 2010). Current retrieval algorithms can struggle due to the requirement for identifying the presence of snow and also correctly accounting for its altered reflectance properties. The surface mines of the AOSR are also surrounded by boreal forest that is associated with a very low reflectance, providing the additional challenge of a changing albedo over a small area.

Therefore, we recalculate the AMFs and examine their impact on the TROPOMI tropospheric NO_2 columns over the AOSR. Similar work has previously been carried out for sensors such as GOME, OMI, and SCIAMACHY that relies on improving the AMFs by regional high-resolution models (e.g., Lin et al., 2014; Martin et al., 2002, 2003; Palmer et al., 2001; Russell et al., 2011; Zhou et al., 2009). The procedure is similar to that from McLinden et al. (2014) with the following differences: (1) GEM-MACH version 2, at 10-km resolution, updated emissions and using output at the time of the satellite overpass was used to provide the NO_2 profile shape; (2) Interactive Multisensor Snow and Ice Mapping System (IMS) (Helfrich et al., 2007) at 4-km resolution was used to flag pixels with snow cover (which has been shown to better identify snow-covered scenes (Cooper et al., 2018; McLinden et al., 2014)); and (3) the use of the SASKTRAN radiative transfer model (Bourassa et al., 2008; Dueck et al., 2017; Zawada et al., 2015) was used for the generation of the AMF lookup tables. SASKTRAN is employed here as it is more readily able to implement future planned improvements such as non-Lambertian surfaces. Aerosols are not considered included in these AMF calculations, similar to the standard TROPOMI AMFs, but are accounted for in the alternative AMF uncertainty budget. The cloud input needed for the estimation is taken from the TROPOMI product ("cloud_fraction_crb_nitrogendioxide_window," "cloud_fraction_crb_nitrogendioxide_window," and "cloud_pressure_crb").

To improve the accuracy of the albedo, we use the Moderate Resolution Imaging Spectroradiometer (MODIS) albedo at a resolution of $0.05 \times 0.05°$ (collection 6.1 MCD43C3; Schaaf et al., 2002). From this, a monthly-mean albedo is computed considering only 100% snow-free pixels, and a climatology of the MODIS albedo is used that only includes pixels with full snow cover (further details can be found in the supporting information).

An uncertainty is estimated for the alternative tropospheric columns (similar to McLinden et al., 2014) by adding the uncertainty of the slant column density (provided in the S5P NO_2 data product), the uncertainty of the stratospheric column density (provided in the S5P NO_2 data product), and the uncertainty of the alternative AMF (assumed to be 20%) in quadrature. The uncertainty of the AMF contains uncertainties from cloud fraction, cloud pressure, albedo, surface pressure, and profile shape (McLinden et al., 2014).

3. TROPOMI Over the Canadian Oil Sands

Before the launch of TROPOMI, OMI has been used extensively to study the distribution and evolution of NO_2 over the Canadian oil sands McLinden et al. (2012, 2016). However, due to the small spatial extent of the surface mining, which is commensurate with OMI's pixel size, it was not possible to observe individual plumes. It was only possible to reliably map the average distribution by considering several years together, and emissions estimates were for the mining region as a whole (Fioletov et al., 2016).

Figures 1a and 1b show TROPOMI and OMI observations for a single day, 9 April 2018, over the AOSR surface mines. TROPOMI shows well-defined plumes of significantly elevated NO_2 originating from two distinct mining areas from which it should be possible to estimate NO_x emissions. From the spatial location of the plumes in Figure 1 a, it appears that the well-defined NO_2 plume in the south originates from the bitumen upgrading stacks that are elevated sources, while the more diffuse enhancement in the north is consistent with the heavy hauler trucks, a surface source. OMI, by contrast, shows much more modest enhancements for about a half-dozen pixels and captures none of the fine details making its spatial distribution impossible to interpret. Averaging TROPOMI over the 3-month period of interest using the oversampling technique of Fioletov et al. (2011) provides a distribution very similar to that of an OMI multiyear average, but with much better resolved spatial patterns and higher peak values (Figures 1c and 1d). The distribution shows a separation of the NO_2 between the northern and southern mines.
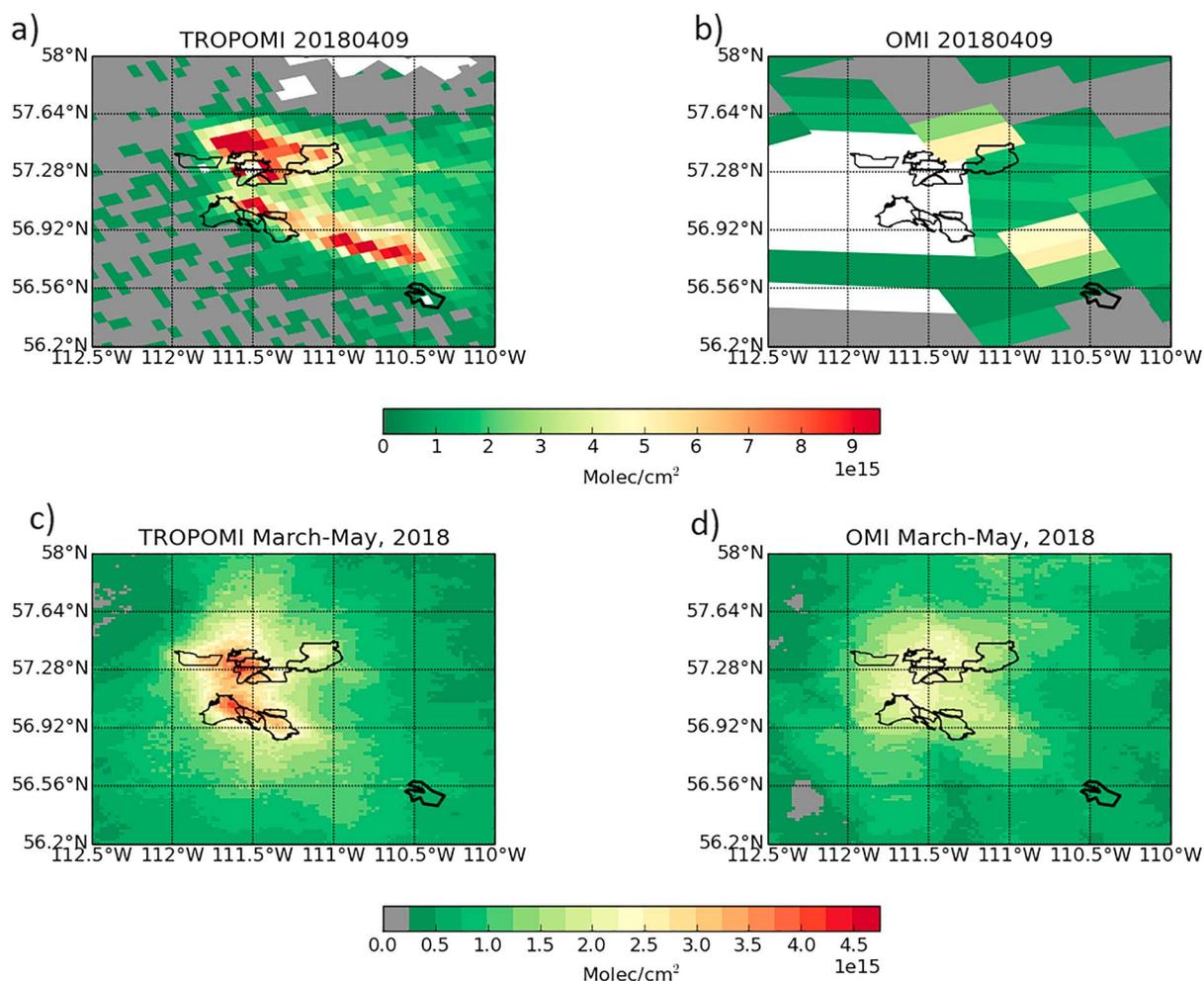
Figure 1. NO_2 measured by (a) TROPOMI and (b) OMI on 9 April 2018 over the surface mines of the Athabasca Oil Sands Region (with NW winds). Averages (March–May 2018) with an averaging radius of 5 and 16 km were used for (c) TROPOMI and (d) OMI, respectively. The black line traces the borders of the individual mining operations. TROPOMI = TROPOspheric Monitoring Instrument; OMI = Ozone Monitoring Instrument.

4. Evaluation of the NO_2 Product

4.1. Spiral Flights

As noted in section 2.2, spirals were flown (within ± 2 hr of the TROPOMI overpass time) with an approximate diameter of 5 km and as high as 2,300 m agl that penetrated the plume top (see Figures S2 and S5 for the horizontal and vertical extend of these spirals). These types of aircraft measurements can be used to estimate the NO_2 VCDs in the PBL and determine AMFs based on the measured NO_2 profiles. Using this true profile to calculate AMFs helps to identify errors in the retrieval and further allows a more quantitative evaluation of AMFs derived using model inputs. The aircraft profile spirals began as low as approximately 200 m agl, measuring volume mixing ratios (VMRs) throughout the PBL. To compare these to TROPOMI, we estimated a tropospheric NO_2 VCD using the aircraft measurements from those spirals. For this estimation, the aircraft measurements are binned into 100-m levels; between the surface and lowest aircraft altitude, we assume a well-mixed layer and use the concentration of the lowest measurements. Above the maximum flight altitude we use NO_2 VMRs from the GEOS-Chem model accounting for $\sim 1.8 \times 10^{14}$ molec/cm^2. Temperatures and pressures needed for the calculation were taken from the operational GEM-MACH model. During the three aircraft flights, seven spirals were flown. Figure 2 a shows the in situ measurements of three spiral flights along with the GEM-MACH NO_2 VMRs (for the nearest grid box at the closest hour). GEM-MACH reproduces the actual NO_2 measurements very well in the PBL, and Figure 2 shows that the profile is captured well by the model. However, it does not always capture the height of the boundary layer, and, as such, there is disagreement above approximately 1.5 km, where NO_2 VMRs drop to near zero in the model.
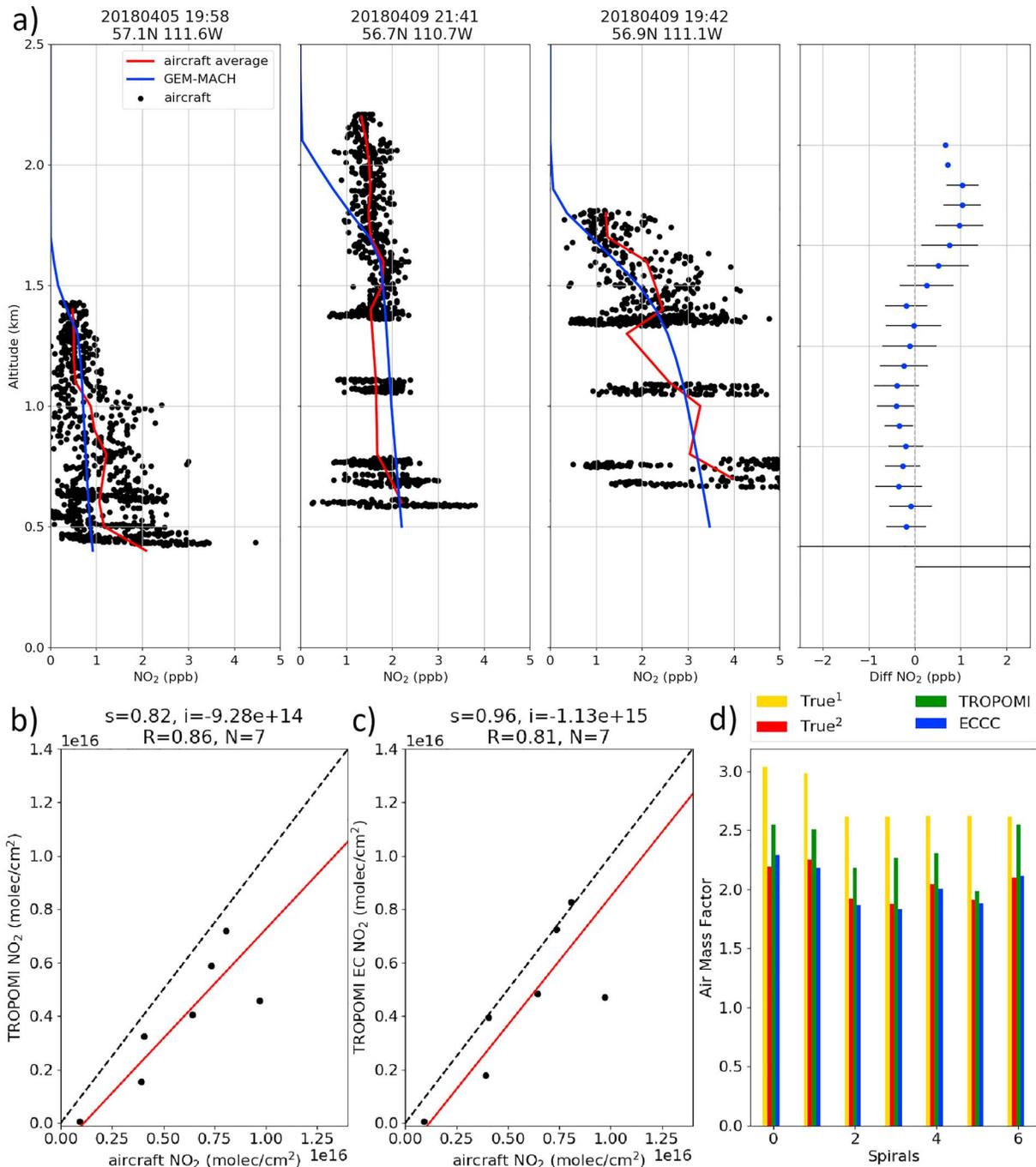
Figure 2. (a) In situ aircraft measurements and GEM-MACH model output of the three of the seven spiral flights that are at least partially covered by retrieved TROPOMI pixels (the location of these spirals can be seen in Figure S2 and the profile of all spirals in Figure S5). The right figure shows the mean difference (and standard deviation) between the GEM-MACH model and the aircraft measurements from all seven spirals. Note that very high and low concentrations can occur in one altitude range as the aircraft flies in and out of plumes. Aircraft columns versus (b) the original and (c) the alternative AMF TROPOMI NO_2 columns. The solid red and the black dashed lines represent the line of best fit and the 1:1 line, respectively. (d) AMFs, including the original TROPOMI (AMF TROPOMI; green), the recalculated (AMF EC; blue), and the calculated "true" AMF from aircraft measurements using the TROPOMI aldebo (true 1; yellow) the MODIS albedo (true 2; red). TROPOMI = TROPOspheric Monitoring Instrument; GEM-MACH = Global Environmental Multiscale-Modelling Air-quality and Chemistry; AMF = air mass factor; ECCC = Environment and Climate Change Canada.
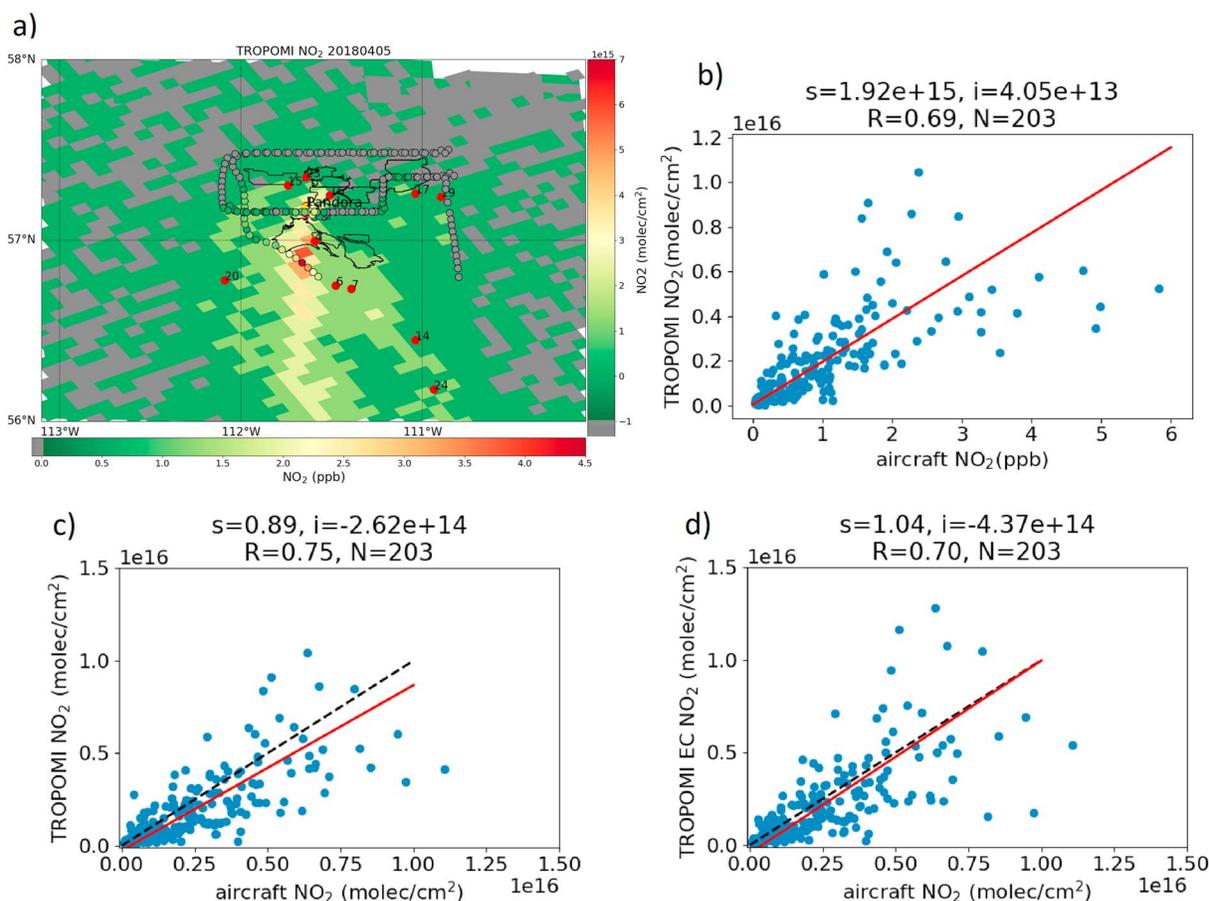
Figure 3. (a) Map around the Athabasca Oil Sands Region showing the NO_2 volume mixing ratios as sampled by the aircraft (for clarity of the plot the averages of 30 data points are shown) and TROPOMI tropospheric NO_2 VCD pixels for 5 April 2018; highlighted are the WBEA stations (in red; the numbers correspond to the station number) and the Pandora location in yellow. TROPOMI tropospheric NO_2 columns versus aircraft in situ measurements (b), the aircraft VCDs (Equation 1) (c), and the aircraft VCDs versus the alternative TROPOMI columns (d). For the regression analysis, we use a geometric mean analysis with $y = sx + i$ (s and i values are indicated in the plots, as well as the correlation coefficient, R, and the number of points, N). TROPOMI = TROPOspheric Monitoring Instrument; VCD = vertical column density.

The comparison with the aircraft spirals indicates a low bias for TROPOMI (approximately −18 % compared to the aircraft measurements). This bias nearly disappears (<5 %) if the alternative AMFs are applied (panel c). Figure 2 d shows the "true" AMF estimated using the albedo as used in the TROPOMI input file (orange), and using the MODIS albedo (red). The comparison (Figure 2 d) shows that the AMFs (using the MODIS albedo) from the aircraft measurements are very close to the estimated AMFs (blue) using the GEM-MACH model and that TROPOMI tropospheric AMFs (green) are likely overestimated in this region (above snow). It also shows that a wrong profile shape over the AOSR and an albedo that is too high can potentially cancel each other's effects, leading to a TROPOMI AMF value close to the "true" AMF (red). This highlights the benefits of using of a high-resolution regional model, which reproduces AMFs close to the true/measured AMFs.

4.2. Spatial Correlation with the Aircraft Measurements
While tropospheric NO_2 VCDs can be estimated from the spirals, only seven spirals are available for comparison with seven TROPOMI NO_2 VCDs that are covered by those spirals. In this section, we evaluate the ability of TROPOMI to detect localized enhancements of tropospheric NO_2 on the scale of its pixel size, using all pixels and aircraft measurements to evaluate the ability of TROPOMI to capture spatial gradients. We average all aircraft in situ measurements of NO_2 for the three flights that are sampled below 1 km agl (to ensure the data collected is in the PBL), taken within ±2 hr within the overpass time, and that are within
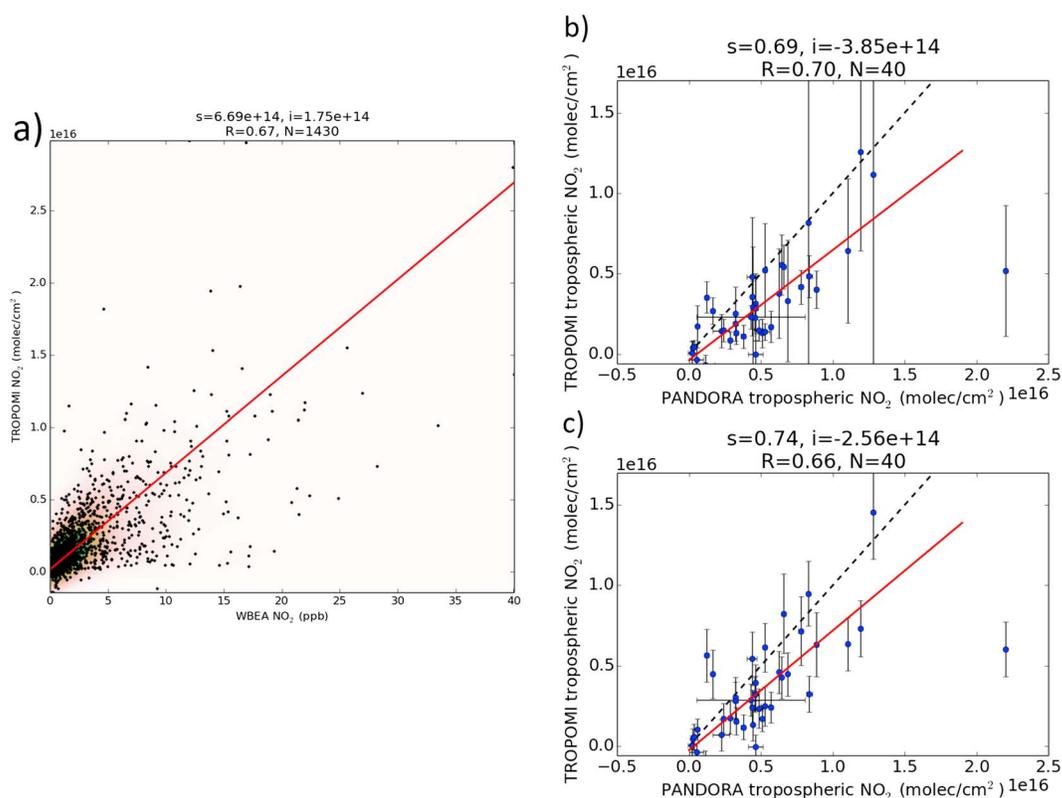
Figure 4. TROPOMI tropospheric NO$_2$ columns versus the ground-based in-situ (a) and remote-sensing Pandora measurements (b-c) for: (b) the original TROPOMI columns, and (c) the alternative columns. TROPOMI = TROPOspheric Monitoring Instrument.

the area of the individual TROPOMI pixel. For all three flights the surface below was covered completely in snow and ice (Figure S2). On average, over 150 aircraft in situ NO$_2$ measurements with an integration time of 3 s were taken within one TROPOMI pixel, and some pixels contain as many as 700. The aircraft in situ and the TROPOMI measurements (Figure 3) correlate well, with a correlation coefficient $R \approx 0.7$, showing that TROPOMI captured the gradients and localized enhancements of NO$_2$ on its small pixel size of approximately 6×7 km^2. To be able to quantitatively compare the satellite VCDs to the in situ VMRs, we convert the average in situ measurements (at the average aircraft altitude, h, below 1,000 m agl) into tropospheric VCDs using the daily output from the GEM-MACH model:

$$\text{VCD}_{aircraft} = \frac{\text{C}_{aircraft}(h)}{\text{C}_{GEM-MACH}(h)} \times \text{VCD}_{GEM-MACH,PBL} + \text{VCD}_{GEOS-Chem,free\,trop}. \tag{1}$$

The results (Figure 3c) indicate a low bias of approximately 15% for the TROPOMI tropospheric NO$_2$ VCDs compared to the aircraft measurements, with a mean difference of $-5.3e14$ molec/cm^2 (-21%; TROPOMI-aircraft) and a random error of approximately 0.97e15 molec/cm^2. After applying the correction to the TROPOMI VCDs (as described in section 2.5), the bias is reduced to 4%, leading to an accuracy of $-3.3e14$ molec/cm^2 (-13%; TROPOMI-aircraft), and a random error of 1.27e15 molec/cm^2. The improved slope in Figure 3d is expected given that the same profile shape is now used for both the scaling of aircraft concentrations and in the calculations of AMFs. The correlation between the aircraft measurements and the TROPOMI retrievals does not improve using the alternative AMFs.

4.3. Comparison With Ground-Based Measurements

To evaluate TROPOMI's ability to capture NO$_2$ distributions over a longer time and spatial scale than that covered by the aircraft flights, comparisons are made with measurements from a ground-based in situ network (WBEA). The results are displayed in Figure 4a for measurements between March and May 2018, comparing the TROPOMI measurements from individual pixels to the averaged WBEA NO$_2$ measurements (± 30 min of the TROPOMI overpass). Only the TROPOMI pixels that cover the stations are used (due to the small size of the TROPOMI pixel and the distance between the WBEA stations, one pixel only usually one

station, sometimes two). Overall, there is a good correlation between the TROPOMI tropospheric VCDs and the surface measurements ($R = 0.67$). To examine the theoretical correlation with surface measurements, we utilize output from an offline run of GEM-MACH at 2.5-km resolution. The correlation between model VCD and model surface VMR without any noise is roughly 0.6 (Figure S7) and only decreases slightly with increased smoothing. Considering the observed correlation, with measurement noise, is comparable to this or slightly higher than that from these noise-free simulations, it appears that the reduction in correlation from unity is mainly due to the mismatch in the qualities being compared (column vs. surface) and little from the noise in either type of observation.

For the comparison with the TROPOMI NO_2 tropospheric columns, we average the Pandora data (± 30 min of the TROPOMI overpass) and subtract the corresponding TROPOMI NO_2 stratospheric columns to obtain a tropospheric Pandora columns. A good agreement was found between the TROPOMI and the Pandora columns (Figure 4b). The theoretical correlation is expected around 0.95 with a slope of 0.85–0.9 at TROPOMI resolution (Figure S7). The regression analysis shows a low bias for the TROPOMI tropospheric NO_2 VCDs with a slope of approximately 0.7. The slope increases to 0.75 when the alternative AMF is applied, which is only 0.1 lower than the expected slope (Figure 4c); the correlation, however, slightly decreases.

While most of the ground in March and April was covered by snow, there are snow-free days at the end of April and in May over the AOSR. However, even for the snow-free days a small low bias of the original TROPOMI NO_2 VCDs remains over the AOSR. Also for snow-free days, we found that the MODIS albedo is approximately half of the climatological OMI albedo used as input for the original AMFs (Figure S4). This low albedo appears to offset the effect of the TM5 model at 1° resolution, which has the effect of diluting emissions and leading to profiles that are not sufficiently weighted to near-surface NO_2. The alternative and original TROPOMI NO_2 VCDs agree within the estimated uncertainties; however, the uncertainties associated with the original NO_2 tropospheric columns, which can be close to 100 % over snow, can be much reduced by higher-resolution input (Figure S6).

5. Discussion and Conclusions

This study presents the first results of TROPOMI NO_2 VCDs over the AOSR. We found that TROPOMI has an outstanding ability to detect tropospheric NO_2 on a very high horizontal resolution. The noise of the individual TROPOMI pixels is quite low, and without averaging there is a high correlation ($R \sim 0.8 - 0.7$) between the TROPOMI observations and the aircraft in situ measurements in the boundary layer that sampled air across the TROPOMI pixels. As promised, the TROPOMI tropospheric NO_2 product can retrieve good quality information on a $6 \times 7\,km^2$ (and even smaller) resolution that is finer than any previous satellites could archive.

Further, TROPOMI displays a high correlation with ground-based in situ and remote sensing measurements that is a clear improvement over previous satellite-remote sensing measurements of NO_2. Its predecessor, OMI (NO_2 SPv3.1), only shows low to moderate correlation with ground-based in situ ($R = 0.35$) and remote-sensing ($R = 0.06$) measurements if the same method is applied (supplementary material). For the ground-based in situ and remote-sensing measurements, there is a good correlation ($R \approx 0.68$) with TROPOMI NO_2. Again, this is a significant improvement to previous satellite and ground-based in situ comparisons where measurements are typically averaged over years to achieve a good correlation (McLinden et al., 2014) or the correlation is moderate ($R \approx 0.4$) if no corrections are applied (Kramer et al., 2008).

Quantitatively, we found a low bias of -15% to -30% of the TROPOMI tropospheric NO_2 columns over the AOSR that was consistent for all of the comparisons carried out in this study. Previously similar discrepancies have been identified for OMI, which were associated with issues of input data used to estimate the tropospheric AMF (McLinden et al., 2014). Here we recalculated the AMFs using higher-resolution input data. This includes, a high-resolution model, GEM-MACH ($10 \times 10\,km^2$ resolution), to estimate the NO_2 profile shape for the lower part of the troposphere, a better identification of snow-covered surfaces (ice mapping system, on $4 \times 4\,km^2$ resolution) and the surface reflectivity from the MODIS satellite. This improved input data provided more precise information on surface cover and more appropriate albedo, if snow is present. Using the alternative tropospheric NO_2 VCDs, the low bias is reduced to between 0% and -25%. Thus, the low bias is not due to the retrieval itself but is associated with the input data used for the tropospheric AMF calculation. A low bias can be seen for both snow-covered and snow-free surfaces, indicating that the issue

is due to both an incorrect albedo over snow and an inaccurate NO_2 profile shape over the AOSR. While using high-resolution input improves the tropospheric AMF and as such the tropospheric NO_2 VCDs, this correction is not as significant as previously seen for OMI (McLinden et al., 2014). For differences where the recalculated NO_2 columns increased by a factor of 2 compared to the original, we only see a 5–15% improvement of the bias when the alternative AMFs were used. Based on our analysis, we recommend to improve the albedo (particularly over snow), as well as the snow flag information for the global product. Second, regional products could be developed, using high-resolution model information to improve the NO_2 a priori. Furthermore, our analysis of the tropospheric columns and the good agreement with other measurements suggest that the TROPOMI stratospheric NO_2 column estimates seem to work well.

Overall, we found that the combination of data quality, noise level, and spatial resolution of these satellite borne NO_2 VCDs is unprecedented and superior to previous sensors. These high-resolution TROPOMI NO_2 observations can allow to pinpoint even kilometer-scale emission sources and estimate localized emissions from industry, cities, or fires on a monthly and likely daily basis.

References

Akingunola, A., Makar, P. A., Zhang, J., Darlington, A., Li, S.-M., Gordon, M., et al. (2018). A chemical transport model study of plume-rise and particle size distribution for the Athabasca oil sands. *Atmospheric Chemistry and Physics*, *18*(12), 8667–8688. https://doi.org/10.5194/acp-18-8667-2018

Bey, I., Jacob, D. J., Yantosca, R. M., Logan, J. A., Field, B. D., Fiore, A. M., et al. (2001). Global modeling of tropospheric chemistry with assimilated meteorology: Model description and evaluation. *Journal of Geophysical Research*, *106*(D19), 23,073–23,095. https://doi.org/10.1029/2001JD000807

Boersma, K. F., Eskes, H. J., & Brinksma, E. J. (2004). Error analysis for tropospheric NO2 retrieval from space. *Journal of Geophysical Research*, *109*, D04311. https://doi.org/10.1029/2003JD003962

Boersma, K. F., Eskes, H. J., Dirksen, R. J., van der A, R. J., Veefkind, J. P., Stammes, P., et al. (2011). An improved tropospheric NO_2 column retrieval algorithm for the Ozone Monitoring Instrument. *Atmospheric Measurement Techniques*, *4*, 1905–1928.

Boersma, K. F., Eskes, H. J., Richter, A., De Smedt, I., Lorente, A., Beirle, S., et al. (2018). Improving algorithms and uncertainty estimates for satellite NO_2 retrievals: Results from the Quality Assurance for Essential Climate Variables (QA4ECV) project. *Atmospheric Measurement Techniques Discussions*, *2018*, 1–70. https://doi.org/10.5194/amt-2018-200

Bourassa, A., Degenstein, D., & Llewellyn, E. (2008). SASKTRAN: A spherical geometry radiative transfer code for efficient estimation of limb scattered sunlight. *Journal of Quantitative Spectroscopy and Radiative Transfer*, *109*(1), 52–73. https://doi.org/10.1016/j.jqsrt.2007.07.007

Bovensmann, H., Burrows, J. P., Buchwitz, M., Frerick, J., Noël, S., Rozanov, V. V., et al. (1999). SCIAMACHY: Mission objectives and measurement modes. *Journal of the Atmospheric Sciences*, *56*(2), 127–150. https://doi.org/10.1175/1520-0469(1999)056<0127:SMOAMM>2.0.CO;2

Burrows, J. P., Weber, M., Buchwitz, M., Rozanov, V., Ladstätter-Weißenmayer, A., Richter, A., et al. (1999). The global Ozone Monitoring Experiment (GOME): Mission concept and first scientific results. *Journal of the Atmospheric Sciences*, *56*(2), 151–175. https://doi.org/10.1175/1520-0469(1999)056<0151:TGOMEG>2.0.CO;2

Callies, J., Corpaccioli, E., Eisinger, M., Hahne, A., & Lefebvre, A. (2000). GOME-2-Metop's second-generation sensor for operational ozone monitoring, 102, 28–36.

Coats, C. J. (1996). High-performance algorithms in the Sparse Matrix Operator Kernel Emissions (SMOKE) Modeling System, American Meteorological Society, Atlanta, GA. USA, proceedings of the Ninth AMS Joint Conference on Applications of Air Pollution Meteorology with AWMA, 28 January–2 February 1996.

Cooper, M. J., Martin, R. V., Lyapustin, A. I., & McLinden, C. A. (2018). Assessing snow extent data sets over North America to inform and improve trace gas retrievals from solar backscatter. *Atmospheric Measurement Techniques*, *11*(5), 2983–2994. https://doi.org/10.5194/amt-11-2983-2018

Côté, J., Gravel, S., Méthot, A., Patoine, A., Roch, M., & Staniforth, A. (1998). The Operational CMC-MRB Global Environmental Multiscale (GEM) Model. Part I: Design Considerations and Formulation. *Monthly Weather Review*, *126*(6), 1373–1395. https://doi.org/10.1175/1520-0493(1998)126<1373:TOCMGE>2.0.CO;2

de Foy, B., Lu, Z., Streets, D. G., Lamsal, L. N., & Duncan, B. N. (2015). Estimates of power plant NO_x emissions and lifetimes from OMI NO_2 satellite retrievals. *Atmospheric Environment*, *116*, 1–11. https://doi.org/10.1016/j.atmosenv.2015.05.056

Dueck, S. R., Bourassa, A. E., & Degenstein, D. A. (2017). An efficient algorithm for polarization in the SASKTRAN radiative transfer framework. *Journal of Quantitative Spectroscopy and Radiative Transfer*, *199*, 1–11. https://doi.org/10.1016/j.jqsrt.2017.05.016

Environment Canada (2018). Air pollution: drivers and impacts. Retrieved from http://www.ec.gc.ca/indicateurs-indicators/default.asp?lang=En&n=D189C09D-1 ; last accessed: 24 September 2018.

Fioletov, V. E., McLinden, C. A., Cede, A., Davies, J., Mihele, C., Netcheva, S., et al. (2016). Sulfur dioxide (SO_2) vertical column density measurements by Pandora spectrometer over the Canadian oil sands. *Atmospheric Measurement Techniques*, *9*(7), 2961–2976. https://doi.org/10.5194/amt-9-2961-2016

Fioletov, V. E., McLinden, C. A., Krotkov, N., Moran, M. D., & Yang, K. (2011). Estimation of SO_2 emissions using OMI retrievals. *Geophysical Research Letters*, *38*, L21811. https://doi.org/10.1029/2011GL049402

Ghude, S. D., Kulkarni, S. H., Jena, C., Pfister, G. G., Beig, G., Fadnavis, S., & van der A, R. J. (2013). Application of satellite observations for identifying regions of dominant sources of nitrogen oxides over the Indian Subcontinent. *Journal of Geophysical Research: Atmospheres*, *118*, 1075–1089. https://doi.org/10.1029/2012JD017811

Girard, C., Plante, A., Desgagné, M., McTaggart-Cowan, R., Côté, J., Charron, M., et al. (2014). Staggered vertical discretization of the Canadian Environmental Multiscale (GEM) Model using a coordinate of the log-hydrostatic-pressure type. *Monthly Weather Review*, *142*(3), 1183–1196. https://doi.org/10.1175/MWR-D-13-00255.1

Health Canada (2018). Human health risk assessment for ambient nitrogen dioxide. Retrieved from https://www.canada.ca/en/health-canada/services/publications/healthy-living/human-health-risk-assessment-ambient-nitrogen-dioxide.html; last accessed: 24 September 2018.

Helfrich, S. R., McNamara, D., Ramsay, B. H., Baldwin, T., & Kasheta, T. (2007). Enhancements to, and forthcoming developments in the Interactive Multisensor Snow and Ice Mapping System (IMS). *Hydrological Processes*, *21*(12), 1576–1586. https://doi.org/10.1002/hyp.6720

Herman, J., Cede, A., Spinei, E., Mount, G., Tzortziou, M., & Abuhassan, N. (2009). NO_2 column amounts from ground-based Pandora and MFDOAS spectrometers using the direct-sun DOAS technique: Intercomparisons and application to OMI validation. *Journal of Geophysical Research*, *114*, D13307. https://doi.org/10.1029/2009JD011848

Hsu, Y.-M., Percy, K., & Hansen, M. (2010). Comparison of passive and continuous measurements of O 3, SO 2 and NO 2 in the Athabasca oil sands region. *Proceedings of the Air and Waste Management Association's Annual Conference and Exhibition, AWMA*, *1*, 804–808.

Hu, H., Landgraf, J., Detmers, R., Borsdorff, T., de Brugh, J. A., Aben, I., et al. (2018). Toward global mapping of methane with TROPOMI: First results and intersatellite comparison to GOSAT. *Geophysical Research Letters*, *45*(8), 3682–3689. https://doi.org/10.1002/2018GL077259

Kleipool, Q. L., Dobber, M. R., de Haan, J. F., & Levelt, P. F. (2008). Earth surface reflectance climatology from 3 years of OMI data. *Journal of Geophysical Research*, *113*, D18308. https://doi.org/10.1029/2008JD010290

Kramer, L. J., Leigh, R. J., Remedios, J. J., & Monks, P. S. (2008). Comparison of OMI and ground-based in situ and MAX-DOAS measurements of tropospheric nitrogen dioxide in an urban area. *Journal of Geophysical Research*, *113*, D16S39. https://doi.org/10.1029/2007JD009168

Krotkov, N. A., Lamsal, L. N., Celarier, E. A., Swartz, W. H., Marchenko, S. V., Bucsela, E. J., et al. (2017). The version 3 OMI NO_2 standard product. *Atmospheric Measurement Techniques*, *10*(9), 3133–3149. https://doi.org/10.5194/amt-10-3133-2017

Krotkov, N. A., McLinden, C. A., Li, C., Lamsal, L. N., Celarier, E. A., Marchenko, S. V., et al. (2016). Aura OMI observations of regional SO_2 and NO_2 pollution changes from 2005 to 2015. *Atmospheric Chemistry and Physics*, *16*(7), 4605–4629. https://doi.org/10.5194/acp-16-4605-2016

Levelt, P. F., van den Oord, G. H. J., Dobber, M. R., Mälkki, A., Visser, H., de Vries, J., et al. (2006). The ozone monitoring instrument. *IEEE Transactions on Geoscience and Remote Sensing*, *44*, 1093–1101.

Lin, J.-T., Martin, R. V., Boersma, K. F., Sneep, M., Stammes, P., Spurr, R., et al. (2014). Retrieving tropospheric nitrogen dioxide from the ozone monitoring instrument: Effects of aerosols, surface reflectance anisotropy, and vertical profile of nitrogen dioxide. *Atmospheric Chemistry and Physics*, *14*(3), 1441–1461. https://doi.org/10.5194/acp-14-1441-2014

Lorente, A., Folkert Boersma, K., Yu, H., Dörner, S., Hilboll, A., Richter, A., et al. (2017). Structural uncertainty in air mass factor calculation for NO_2 and HCHO satellite retrievals. *Atmospheric Measurement Techniques*, *10*(3), 759–782. https://doi.org/10.5194/amt-10-759-2017

Lu, Z., & Streets, D. G. (2012). Increase in NO_x emissions from Indian thermal power plants during 1996–2010: Unit-based inventories and multisatellite observations. *Environmental Science & Technology*, *46*(14), 7463–7470. https://doi.org/10.1021/es300831w

Makar, P., Gong, W., Hogrefe, C., Zhang, Y., Curci, G., Zabkar, R., et al. (2015). Feedbacks between air pollution and weather, part 2: Effects on chemistry. *Atmospheric Environment*, *115*, 499–526. https://doi.org/10.1016/j.atmosenv.2014.10.021

Makar, P., Gong, w., Milbrandt, J., Hogrefe, C., Zhang, Y., Curci, G., et al. (2015). Feedbacks between air pollution and weather, Part 1: Effects on weather. *Atmospheric Environment*, *115*, 442–469.

Marchenko, S., Krotkov, N. A., Lamsal, L. N., Celarier, E. A., Swartz, W. H., & Bucsela, E. J. (2015). Revising the slant column density retrieval of nitrogen dioxide observed by the ozone monitoring instrument. *Journal of Geophysical Research: Atmospheres*, *120*, 5670–5692. https://doi.org/10.1002/2014JD022913

Martin, R. V., Chance, K., Jacob, D. J., Kurosu, T. P., Spurr, R. J. D., Bucsela, E., et al. (2002). An improved retrieval of tropospheric nitrogen dioxide from GOME. *Journal of Geophysical Research*, *107*(D20), ACH 9–1-ACH 9–21. https://doi.org/10.1029/2001JD001027

Martin, R. V., Jacob, D. J., Chance, K., Kurosu, T. P., Palmer, P. I., & Evans, M. J. (2003). Global inventory of nitrogen oxide emissions constrained by space-based observations of NO_2 columns. *Journal of Geophysical Research*, *108*(D17), 4537. https://doi.org/10.1029/2003JD003453

McLinden, C. A., Fioletov, V., Boersma, K. F., Kharol, S. K., Krotkov, N., Lamsal, L., et al. (2014). Improved satellite retrievals of NO_2 and SO_2 over the Canadian oil sands and comparisons with surface measurements. *Atmospheric Chemistry and Physics*, *14*(7), 3637–3656. https://doi.org/10.5194/acp-14-3637-2014

McLinden, C. A., Fioletov, V., Boersma, K. F., Krotkov, N., Sioris, C. E., Veefkind, J. P., & Yang, K. (2012). Air quality over the Canadian oil sands: A first assessment using satellite observations. *Geophysical Research Letters*, *39*, L04804. https://doi.org/10.1029/2011GL050273

McLinden, C. A., Fioletov, V., Krotkov, N. A., Li, C., Boersma, K. F., & Adams, C. (2016). A decade of change in NO_2 and SO_2 over the Canadian Oil Sands as seen from space. *Environmental Science & Technology*, *50*(1), 331–337. https://doi.org/10.1021/acs.est.5b04985

Moran, M. D., Ménard, S., Talbot, D., Huang, P., Makar, P. A., Gong, W., et al. (2010). *Particulate-matter forecasting with GEM-MACH15, A New Canadian Air-quality Forecast Model, in: Air pollution modelling and its application XX*. Dordrecht, the Netherlands: Springer.

Noxon, J. F. (1975). Nitrogen dioxide in the stratosphere and troposphere measured by ground-based absorption spectroscopy. *Science*, *189*(4202), 547–549. https://doi.org/10.1126/science.189.4202.547

O'Byrne, G., Martin, R. V., van Donkelaar, A., Joiner, J., & Celarier, E. A. (2010). Surface reflectivity from the Ozone Monitoring Instrument using the Moderate Resolution Imaging Spectroradiometer to eliminate clouds: Effects of snow on ultraviolet and visible trace gas retrievals. *Journal of Geophysical Research*, *115*, D17305. https://doi.org/10.1029/2009JD013079

Palmer, P. I., Jacob, D. J., Chance, K., Martin, R. V., Spurr, R. J. D., Kurosu, T. P., et al. (2001). Air mass factor formulation for spectroscopic measurements from satellites: Application to formaldehyde retrievals from the Global Ozone Monitoring Experiment. *Journal of Geophysical Research*, *106*(D13), 14,539–14,550. https://doi.org/10.1029/2000JD900772

Pendlebury, D., Gravel, S., Moran, M. D., & Lupu, A. (2018). Impact of chemical lateral boundary conditions in a regional air quality forecast model on surface ozone predictions during stratospheric intrusions. *Atmospheric Environment*, *174*, 148–170. https://doi.org/10.1016/j.atmosenv.2017.10.052

Percy, K. E. (2013). Geoscience of climate and energy 11. Ambient air quality and linkage to ecosystems in the Athabasca Oil Sands, Alberta. *Geosciences Canada*, *40*(3), 182–201. https://doi.org/10.12789/geocanj.2013.40.014

Percy, K. E., Hansen, M. C., & Dann, T. (2012). *Air quality in the Athabasca Oil Sands Region, in volume 11: Alberta Oil Sands—Energy, industry and the environment* (1st ed.). New York: Elsevier.

Phillips, D. (2010). The WBEA air quality monitoring network: History of operation and current status. https://doi.org/2010-A-914-AWMA

Platt, U., & Stutz, J. (2008). *Differential optical absorption spectroscopy: Principles and applications*. Berlin, Germany: Springer.

Russell, A. R., Perring, A. E., Valin, L. C., Bucsela, E. J., Browne, E. C., Wooldridge, P. J., & Cohen, R. C. (2011). A high spatial resolution retrieval of NO_2 column densities from OMI: Method and evaluation. *Atmospheric Chemistry and Physics*, *11*(16), 8543–8554. https://doi.org/10.5194/acp-11-8543-2011

Schaaf, C. B., Gao, F., Strahler, A. H., Lucht, W., Li, X., Tsang, T., et al. (2002). First operational BRDF, albedo nadir reflectance products from MODIS. *Remote Sensing of Environment*, *83*(1), 135–148. https://doi.org/10.1016/S0034-4257(02)00091-3, the Moderate Resolution Imaging Spectroradiometer (MODIS): A new generation of Land Surface Monitoring.

Sioris, C. E., McLinden, C. A., Shephard, M. W., Fioletov, V. E., & Abboud, I. (2017). Assessment of the aerosol optical depths measured by satellite-based passive remote sensors in the Alberta oil sands region. *Atmospheric Chemistry and Physics*, *17*(3), 1931–1943. https://doi.org/10.5194/acp-17-1931-2017

U.S. Environmental Protection Agency (1975). Technical assistance document for the chemiluminescence measurement of nitrogen dioxide (*technical report*). Environmental Monitoring and Support Laboratory. Research Triangle Park, North Carolina. Retrieved from https://www3.epa.gov/ttnamti1/archive/files/ambient/criteria/reldocs/4-75-003.pdf

van Geffen, J. H. G. M., Boersma, K. F., Van Roozendael, M., Hendrick, F., Mahieu, E., De Smedt, I., et al. (2015). Improved spectral fitting of nitrogen dioxide from OMI in the 405–465 nm window. *Atmospheric Measurement Techniques*, *8*(4), 1685–1699. https://doi.org/10.5194/amt-8-1685-2015

van Geffen, J. H. G. M., Eskes, H. J., Boersma, K. F., Maasakkers, J. D., & Veefkind, J. P. (2018). *TROPOMI ATBD of the total and tropospheric NO_2 data products* (issue 1.2.0). Royal Netherlands Meteorological Institute (KNMI), De Bilt, the Netherlands, s5P-KNMI-L2-0005-RP.

Veefkind, J., Aben, I., McMullan, K., Forster, H., de Vries, J., Otter, G., et al. (2012). TROPOMI on the ESA Sentinel-5 Precursor: A GMES mission for global observations of the atmospheric composition for climate, air quality and ozone layer applications. *Remote Sensing of Environment*, *120*, 70–83. https://doi.org/10.1016/j.rse.2011.09.027, the Sentinel Missions - New Opportunities for Science.

Williams, J. E., Boersma, K. F., Le Sager, P., & Verstraeten, W. W. (2017). The high-resolution version of TM5-MP for optimized satellite retrievals: description and validation. *Geoscientific Model Development*, *10*(2), 721–750. https://doi.org/10.5194/gmd-10-721-2017

Zara, M., Boersma, K. F., De Smedt, I., Richter, A., Peters, E., van Geffen, J. H. G. M., et al. (2018). Improved slant column density retrieval of nitrogen dioxide and formaldehyde for OMI and GOME-2A from QA4ECV: Intercomparison, uncertainty characterisation, and trends. *Atmospheric Measurement Techniques*, *11*(7), 4033–4058. https://doi.org/10.5194/amt-11-4033-2018

Zawada, D. J., Dueck, S. R., Rieger, L. A., Bourassa, A. E., Lloyd, N. D., & Degenstein, D. A. (2015). High-resolution and monte carlo additions to the Sasktran radiative transfer model. *Atmospheric Measurement Techniques*, *8*(6), 2609–2623. https://doi.org/10.5194/amt-8-2609-2015

Zhang, J., Moran, M. D., Zheng, Q., Makar, P. A., Baratzadeh, P., Marson, G., et al. (2018). Emissions preparation and analysis for multiscale air quality modeling over the Athabasca Oil Sands Region of Alberta, Canada. *Atmospheric Chemistry and Physics*, *18*(14), 10,459–10,481. https://doi.org/10.5194/acp-18-10459-2018

Zhou, Y., Brunner, D., Boersma, K. F., Dirksen, R., & Wang, P. (2009). An improved tropospheric NO_2 retrieval for OMI observations in the vicinity of mountainous terrain. *Atmospheric Measurement Techniques*, *2*(2), 401–416. https://doi.org/10.5194/amt-2-401-2009